ARTICLE

OBC
www.rsc.org/obc

Arginine magic with new counterions up the sleeve

Masamichi Nishihara,[a] Florent Perret,[a] Toshihide Takeuchi,[b] Shiroh Futaki,[b,c] Adina N. Lazar,[d] Anthony W. Coleman,[d] Naomi Sakai*[a] and Stefan Matile*[a]

[a] *Department of Organic Chemistry, University of Geneva, Geneva, Switzerland*
[b] *Institute for Chemical Research, Kyoto University, Japan*
[c] *PRESTO, JST, Kyoto, Japan*
[d] *Institut de Biologie et Chimie des Protéines, CNRS UMR 5086, 7 passage du Vercors, F69367, Lyon, France. E-mail: naomi.sakai@chiorg.unige.ch, stefan.matile@chiorg.unige.ch; Fax: +41(0)22 379 3215; Tel: +41(0)22 379 6523*

Received 28th January 2005, Accepted 4th March 2005
First published as an Advance Article on the web 7th April 2005

The elusive questions how arginine-rich sequences allow peptides and proteins to penetrate cells or to form voltage-gated ion channels are controversial topics of current scientific concern. The possible contributions of exchangeable counterions to these puzzling processes remain underexplored. The objective of this report is to clarify scope and limitations of certain counteranions to modulate cellular uptake and anion carrier activity of oligo/polyarginines. The key finding is that the efficiency of counteranion activators depends significantly on many parameters such as activator–membrane and activator–carrier interactions. This finding is important because it suggests that counteranions can be used to modulate not only efficiency but also selectivity. Specifically, activator efficiencies are found to increase with increasing aromatic surface of the activator, decreasing size of the transported anion, increasing carrier concentration as well as increasing membrane fluidity. Efficiency sequences depend on membrane composition with coronene > pyrene ≫ fullerene > calix[4]arene carboxylates in fluid and crystalline DPPC contrasting to fullerene > calix[4]arene ≈ coronene > pyrene carboxylates in EYPC with or without cholesterol or ergosterol. In HeLa cells, the efficiency of planar activators (pyrene) exceeds that of spherical activators (fullerenes, calixarenes). Polyarginine complexes with pyrene and coronene activators exhibit exceptional excimer emission. Decreasing excimer emission with increasing ionic strength reveals dominant hydrophobic interactions with the most efficient carboxylate activators. Dominance of ion pairing with the inefficient high-affinity sulfate activators is corroborated by the reversed dependence on ionic strength. These findings on activator–carrier and activator–membrane interactions are discussed as supportive of arene-templated guanidinium–carboxylate pairing and interface-directed translocation as possible origins of the superb performance of higher arene carboxylates as activators.

1 Introduction

Arginine-rich peptides and proteins seem to exist always in "functional symbiosis" with tightly bound but exchangeable counteranions. This "counteranion scavenging" could be the trick of oligoarginines to minimize intramolecular charge repulsion (Fig. 1A), because the weak acidity of the guanidinium cation hinders partial deprotonation under physiological conditions.[1] More acidic oligoamines such as K-rich peptides do not show similar affinity to anions (Fig. 1B). Recently, we suggested that counteranion scavenging may explain some of the "mysterious" functions of arginine-rich peptides and proteins in biomembranes.[1] The movement of R-rich cell-penetrating peptides (CPPs) like oligoarginines across bilayer membranes can, for example, be understood as repeated alterations in their solubility by multiple counteranion exchange to adapt to changing environments.[1,2] In support of this hypothesis, it was not surprising to find that a) CPPs are anion carriers and b) that bilayer penetration by CPPs can be regulated with amphiphilic anions (Fig. 2).[1,2] Counteranions (*i.e.*, alignable dipoles of hydrophobic ion pairs) might contribute to the mechanism of voltage gating by R-rich motifs for the same reasons.[1,3–8]

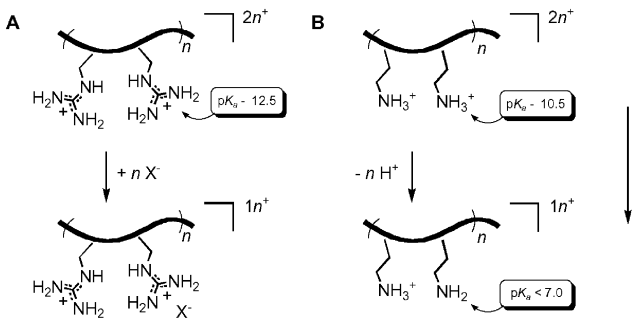

Fig. 1 To minimize repulsion between proximal charges, (A) guanidinium-rich oligomers scavenge anions X^- to give complexes $\mathbf{R}_n \cdot (X)_m$ (Fig. 2), whereas (B) ammonium-rich oligomers release protons.

In our earlier studies, activator anions like EYPG are used as a component of the model membranes.[1,2] Very recently, however, we found that externally added amphiphilic anions **Y** can activate oligo/polyarginine-anion complexes in live cells as well as otherwise inaccessible neutral EYPC bilayers (Fig. 3).[9] Confirmed key characteristics of activators **Y** include one or more negative charge for ion pairing with guanidinium cations of the oligo/polyarginine.[9] Moreover, all anion activators **Y** known so far are amphiphiles with large hydrophobic domains for favorable interactions with the bilayer membrane. Activators **Y** with hydrophobic domains composed of higher aromatics appear particularly promising because additional, more specific activator–carrier, activator–activator and activator–membrane interactions become possible (see below).

Fig. 2 summarizes how activating and inactivating counteranions may contribute to the function of CPPs. In brief, R-rich CPPs $\mathbf{R}_n$ will always exist as complexes $\mathbf{R}_n \cdot (X)_m$ to minimize intramolecular charge repulsion (Fig. 1A). As an illustrative example for the need for counterions, we recently found that oligoarginines can scavenge inorganic phosphates that are present in trace amounts in the environment.[10] Exchange of scavenged hydrophilic counteranions X such as inorganic phosphates in complexes $\mathbf{R}_n \cdot (X)_m$ with activators **Y** is expected to yield active complexes $\mathbf{R}_n \cdot (X)_{m'} \cdot (\mathbf{Y})_{m''}$ at the

DOI: 10.1039/b501472g

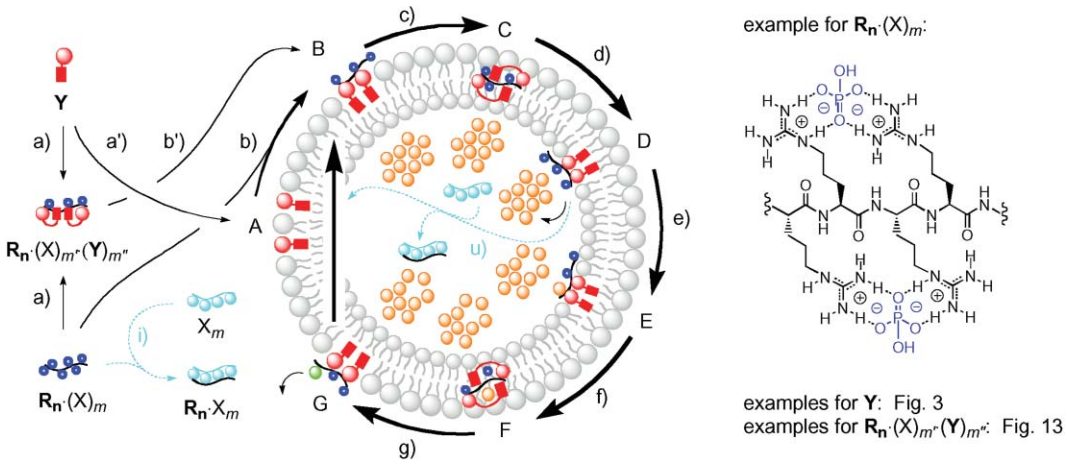

Fig. 2 Counteranion activators **Y** (red) of oligo/polyarginine carriers/CPPs $\mathbf{R}_n$ (black) are thought to act by replacing scavenged hydrophilic anions X (blue) in complexes $\mathbf{R}_n\cdot(X)_m$ to produce complexes $\mathbf{R}_n\cdot(X)_{m'}\cdot(\mathbf{Y})_{m''}$ (B) that act as carriers to release entrapped anions like CF (orange→green, B→G) or are directed by internal or external hydrophilic polyanions X_m (cyan) to accumulate inside (u, uptake) or outside a spherical bilayer membrane (i, inhibition).[1,2]

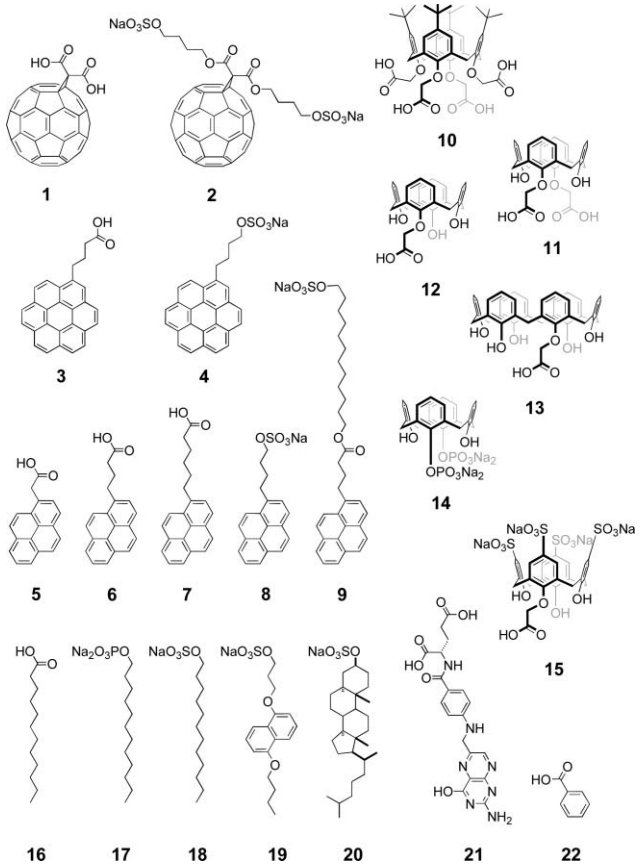

Fig. 3 Structure of potential anion activators **Y** (Fig. 2; anions **14, 15, 21** and **22** are inactive under the employed experimental conditions).

membrane–water interface (Fig. 2B). The resulting supramolecular carriers $\mathbf{R}_n\cdot(X)_{m'}\cdot(\mathbf{Y})_{m''}$ may then shuttle across the bilayer, pick up entrapped anions like CF, back-transfer and release unquenched CF (Fig. 2). Therefore, an efficient activator **Y** should have the ability to form stable but labile guanidinium–anion interactions. Hydrophilic high-affinity polyanions X_m like glycosaminoglycans (GAGs),[1,2] oligonucleotides (RNA, DNA), micelles (SDS)[1,2] and presumably also nucleotides like ATP[1] may play the interesting role to regulate carrier activity and cell penetration. Namely, external X_m should inhibit both processes, whereas internal X_m should inhibit back transfer and thus facilitate the translocation. The possibly more complex role of interfacial polyelectrolytes, particularly GAGs, is a topic of current scientific concern.[11–24] We reiterate that the synergistic carrier mechanism for CPP-activator complexes $\mathbf{R}_n\cdot(X)_{m'}\cdot(\mathbf{Y})_{m''}$ outlined in Fig. 2 is assumed in this report based on results reported in references 1 and 2 that disfavor formation of ion channels and pores as well as the occurrence of more drastic events. Nevertheless, this assumption as well as its relevance for oligo/polyarginine uptake by live cells remains to be verified. Extensive experimental evidence from many groups in support of a carrier but also of other, competing or coinciding uptake mechanisms, particularly endocytosis, exists.[7,8,11–24]

The here envisioned role of CPP activators is reminiscent of the role of charge-reversal amphiphiles in gene delivery.[25–27] The rare occurrence of intrinsic cationic activators in the biomembranes practically excludes spontaneous oligonucleotide translocation, a fact that naturally directs scientific attention to artificial countercation activators. In contrast, ubiquitous anionic activators in biomembranes may have shifted the focus of CPP research from counteranion activators to a mysteriously "spontaneous" uptake[1,2,7,8,11–24] that is sometimes referred to as "arginine magic".

This study focuses on nature and selectivity of the interactions between anion activators, polyarginine (pR) carriers and lipid bilayer membranes. The key question to address was why higher arenes and carboxylates emerge as privileged motifs in efficient activators. With regard to activator–membrane interactions, it is well known that many membrane-spanning proteins exhibit external surfaces with aromatic rings positioned to interact with the interfacial region of bilayer membranes.[28–37] This interface contains the lipidic ester groups as well as their phosphates paired with counterions such as the ammonium cation in the case of phosphatidylcholine. Examples for membrane peptides and proteins with aromatic rings at the interface include β-helices with gramicidin A,[36] α-helix bundles with potassium channels[30] and β-barrels with maltoporin.[28] Model studies confirmed preferential location of indoles at the interface.[31–35] Hydrogen bonding to interfacial esters and cation–π interactions with ammonium cations (but not yet arene-templated ion pairing)[38] have been considered beyond simple preference for intermediate dielectrics to explain interfacial accumulation of arenes.[28–35]

Model studies confirmed that appropriately positioned aromatics can stabilize transmembrane orientation of model helices.[32–34] A similar anchoring function has been proposed for aromatics in synthetic ion channels and pores.[36,37] Important for this study, it has been suggested that the interfacial preference of arenes may drive the translocation across bilayer membranes to interfaces at the other side.[29] For carriers, preferential

accumulation at the interface is essential for function because this is the place where the ions are exchanged. Indeed, we have recently found that interfacial preference is one of the distinguishing characteristics of octaarginine, an excellent CPP, compared to hexadecaarginine, a poor CPP that accumulates in the hydrophobic core of EYPC/EYPG membranes.[2] Therefore, it was conceivable that fullerene, coronene and calixarene activators may preferentially accumulate at the interfacial region and, therefore, mediate interface-directed translocation of polyarginine carriers.

With regard to activator–carrier interactions, Thompson and Smithrud pointed out recently that arene-templated ion pairing occurs in nature and created an elegant synthetic model to secure experimental evidence for relevance of this recognition motif in water and in octanol.[38] Important in the context of this study, the Thompson–Smithrud model identified guanidinium–carboxylate pairs[39–45] as privileged motif; alkyl-templated ion pairing was not observed.[38] Arene-templated ion pairing was explored in the context of α-helix recognition as well.[45] We have proposed the same effect early on as a possible origin of activator–carrier interactions.[1] With respect to the well-recognized cation–π interaction,[46,47] arene-templated ion pairing may be considered as an extension that covers the counteranion and the resulting network of possible interactions between anion, cation and arene as well. Such an influence of a remote[48] aromatic surface to the binding could be the key to achieve stable complexes $pR{\cdot}(X)_{m'}{\cdot}(\mathbf{Y})_{m''}$ with kinetic lability.

Taken together, these considerations suggested that the most efficient activators may bind to CPPs by arene-templated carboxylate–guanidinium pairing to subsequently mediate the interface-directing translocation of the resulting activator–carrier complexes. The studies on activator–membrane and activator–carrier interactions described in the following are in support of this hypothesis, although the involvement of the other mechanisms is likely.

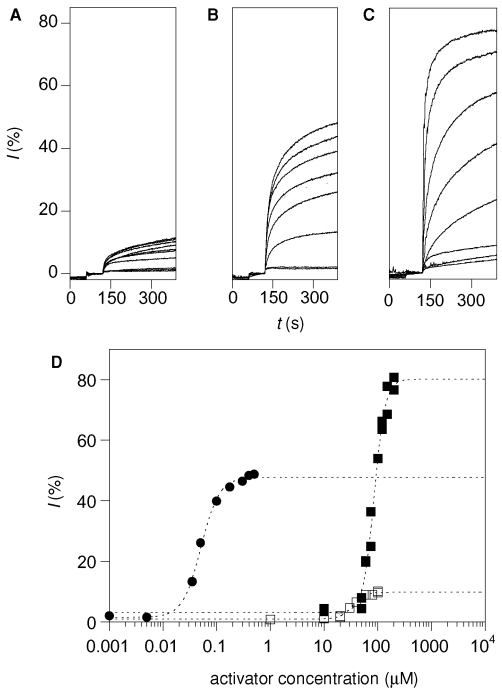

Fig. 4 Activators with poor efficiency (A), superb EC_{50} (B), and superb Y_{MAX} (C) exemplified with laurate **16** (A), fullerene malonate **1** (B) and pyrene acetate **5** (C), measured at 25 °C. (D) Dose response curves for **16** (□), **1** (●) and **5** (■) with curve fit to Hill equation. (A–C): Changes in CF emission I (λ_{ex} 492 nm, λ_{em} 517 nm) as a function of time during addition of activator (at $t = 60$ s; with increasing intensity at $t = 360$ s, 0, 10, 20, 30, 40, 50, 60, 70, 80 and 100 μM **16** in A, 0, 5, 35, 50, 100, 200, 300 and 400 nM **1** in B, 0, 10, 50, 60, 75, 100, 150 and 200 μM **5** in C) and pR (at $t = 120$ s, 250 nM) to EYPC-LUVs⊃CF (250 μM EYPC), calibrated by final lysis ($I = 100\%$ with excess triton X-100).

2 Results and discussion

2.1 The efficiency sequence in EYPC membranes

Anions **1–22** were considered as activators **Y** of polyarginine (pR) to give functional activator–carrier complexes $pR{\cdot}(X)_{m'}{\cdot}(\mathbf{Y})_{m''}$ (Fig. 3). Fullerene (**2**) and coronene (**4**) sulfates were prepared in a few routine steps from commercial starting materials (see Experimental section). Fullerene (**1**) and coronene (**3**) carboxylates as well as calixarene (**8–15**) and naphthalene **19** activators were synthesized following reported procedures.[9] Anions **5–7, 16–18**, and **20–22** were commercially available.

The classical CF assay, in which the release of self-quenched CF from EYPC-LUVs⊃CF is monitored continuously as an increase of fluorescence, was used to assess the ability of amphiphilic anions **1–22** to activate polyarginine carriers pR in otherwise inaccessible, neutral EYPC bilayers.[9] Conventionally, the CF assay is used to identify large pores and membrane-disruptive detergents.[36] However, recent mechanistic studies suggest that oligo-/polyarginines act as anion carriers under the selected conditions,[1,2] although contributions from transient pores and other mechanisms cannot be excluded.[36] In any case, elucidation of the transport mechanism of activator–polyarginine complexes $pR{\cdot}(X)_{m'}{\cdot}(\mathbf{Y})_{m''}$ is not the topic of this study.

Amphiphilic anions **1–22** stimulated pR-mediated CF release from EYPC-LUVs⊃CF in varying extent. Pyreneacetate[49,50] **5**, on the one hand, formed complexes $pR{\cdot}(X)_{m'}{\cdot}(\mathbf{5})_{m''}$ that mediated up to 80% CF release at relatively high concentrations (Fig. 4C and 4D, ■). Complexes $pR{\cdot}(X)_{m'}{\cdot}(\mathbf{1})_{m''}$ with the Bingel fullerene[27,51–56] **1** as an activator, on the other hand, mediated up to 50% CF release at exceptionally low concentrations (Fig. 4B and 4D, ●). Laurate complexes $pR{\cdot}(X)_{m'}{\cdot}(\mathbf{16})_{m''}$,[8] finally, mediated up to 10% CF release only at relatively high concentrations (Fig. 4A and 4D, □). These diverse, in part complementary characteristics of anion activators **1–22** were classified using two parameters: The maximal activity Y_{MAX} and the EC_{50} (Table 1). The effective activator concentration EC_{50} is defined as activator concentration needed to reach $Y_{MAX}/2$ (Table 1). As a general trend, EC_{50}'s decreased with decreasing Y_{MAX}. This was regrettable because the perfect activator should achieve high Y_{MAX} at low EC_{50}. To illustrate this dilemma, activator efficiency E was defined as in eqn. (1) based on the roughly exponential Y_{MAX}–EC_{50} profile[9] of the pyrene series **5–9**. Namely,

$$E = Y_{MAX} \times pEC_{50}/f \quad (1)$$

where Y_{MAX} is the maximal activity in percent, pEC_{50} the negative logarithm of the effective concentration in mM, and $f = 20.6$ an arbitrary scaling factor to calibrate E in EYPC bilayers between 0 and 10. This definition assigned $E = 10$ to the best activator in EYPC bilayers, *i.e.*, the Bingel fullerene **1**. The "pyrene threshold"[9] was located between $E = 4.1$ for **5** and $E = 5.9$ for **9**, *i.e.*, around $E \approx 5.0$.

Only a few anion activators other than fullerene **1** ($E = 10$) exhibited efficiencies clearly above the pyrene threshold: calix[4]arenes[57] **12** ($E = 8.3$), **11** ($E = 7.2$) and **10** ($E = 6.5$) as well as coronenebutyrate[58] **3** ($E = 7.5$). Amphiphilic carboxylates (fullerene ≫ calix[4]arene ≈ coronene > pyrene ≈ steroid > calix[6]arenes > naphthalene[59,60] ≈ alkane) were clearly more efficient than the corresponding sulfates (Table 1) and alcohols (all inactive). Despite promising activity observed with alkyl phosphate (Table 1, entry 17), phosphate activators were not further investigated because of the inactivity of calix[4]arene **14** (Table 1, entry 14).

With 250 nM polymer, the average concentration of guanidinium cations calculated to 18 μM. This suggested that the EC_{50} of most activators was below stoichiometric ion pairing.

Table 1 Characteristics of anion activators **1–22** in EYPC-LUVs⊃CF at constant lipid and carrier concentration[a]

Entry	Anion[b]	Y_{MAX} (%)[c,d]	EC_{50}/μM[c,e]	E[f]
01	**1**	48 ± 1	0.051 ± 0.002	10.0
02	**2**	30 ± 2	0.11 ± 0.006	5.8
03	**3**	65 ± 2	4.3 ± 0.3	7.5
04	**4**	50 ± 3	7.5 ± 0.7	5.2
05	**5**	80 ± 3	86 ± 3	4.1
06	**6**	78 ± 2	44 ± 2	5.1
07	**7**	55 ± 4	9.3 ± 0.7	5.4
08	**8**	48 ± 3	6.7 ± 0.6	5.1
09	**9**	46 ± 2	2.2 ± 0.2	5.9
10	**10**	46 ± 3	1.2 ± 0.2	6.5
11	**11**	65 ± 2	5.3 ± 0.3	7.2
12	**12**	68 ± 2	3.1 ± 0.2	8.3
13	**13**	33 ± 3	5.1 ± 0.4	3.7
14	**14**	—[g]	>100	0.0
15	**15**	—[g]	>100	0.0
16	**16**	10 ± 1	34 ± 1	0.7
17	**17**	61 ± 3	19 ± 1	5.1
18	**18**	27 ± 1	16 ± 1	2.4
19	**19**	30 ± 1	18 ± 1	2.5
20	**20**	48 ± 1	9.3 ± 0.3	4.7
21	**21**	—[g]	>100	0.0
22	**22**	—[g]	>100	0.0

[a] From CF efflux from LUVs⊃CF (250 μM lipid), 250 nM pR, 10 mM $Na_mH_nPO_4$, 100 mM KCl, pH 6.5, 25 °C (if not otherwise indicated); part of the data in Table 1 has been communicated previously in ref. 9. [b] See Fig. 1 for structures. [c] From Hill analysis of dose response curves (*e.g.*, Fig. 4D), see experimental part. [d] Maximal activity at saturation with activator. [e] Effective concentration of anions **1–22** to mediate 50% of maximal activity ($Y_{MAX}/2$). [f] Activator efficiency, eqn. (1). [g] No activity observed.

Remarkably, the EC_{50} of fullerenes **1** (51 nM) and **2** (110 nM) was below the binding of one activator per carrier (250 nM). In other words, fullerenes activators appeared to act at "catalytic" concentrations. "Catalytic" activator efficiency demonstrated that activator–carrier complexes $pR\cdot(X)_{m'}\cdot(\mathbf{1})_{m''}$ form cooperatively as well as that they are active at extremely low concentrations.

Activator efficiency decreased with decreasing carrier concentration. The decrease in Y_{MAX} of coronene carboxylate **3** with decreasing pR concentration, for instance, contributed more to activator efficiency than the compensating decrease in EC_{50} (Fig. 5). The same trend was observed with the less efficient coronene sulfate activator **4** (Table 2).

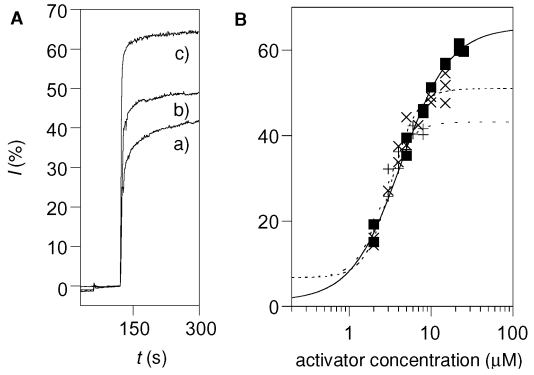

Fig. 5 Dependence of activator efficiency on carrier concentration at 25 °C. (A) Original curves for maximal activity at saturation with coronene activator **3** (added at $t = 60$ s) for (a) 50 nM, (b) 125 nM and (c) 250 nM polyarginine (added at $t = 120$ s, procedure as in Fig. 4). (B) Dose response curves for coronene activator **3** at polyarginine concentrations of 50 nM (+), 125 nM (×) and 250 nM (■).

Transport of anions as large as CF by supramolecular carriers $\mathbf{R}_n\cdot(X)_{m'}\cdot(\mathbf{Y})_{m''}$ was remarkable. However CPPs have been reported to mediate the uptake of even larger objects such as proteins, liposomes or even nanoparticles.[1,2,7,8,11–24] For this reason, it was of interest to see whether or not complexes $pR\cdot(X)_{m'}\cdot(\mathbf{Y})_{m''}$ could mediate the release of anions larger than CF from EYPC LUVs. This question was addressed using CFD, *i.e.*, CF-dextran, a classical probe in size exclusion experiments.[61] CFD release from EYPC-LUVs⊃CFD by pR anion complexes was tested at concentrations above their EC_{50} for CF release from EYPC-LUVs⊃CF (Table 1). Overall poor efficiencies were found for the release of CFD compared to CF (Fig. 6). Highest efficiency to stimulate pR-mediated translocation of large anions was found for planar coronene and pyrene carboxylates **3** and **6**, whereas amphiphilic sulfates were inactive. Highest size selectivity was observed for the more spherical calix[4]arene activator **10** and pyrene hexanoate **7** with poor efficiency to stimulate CFD release (Fig. 6) but acceptable efficiency with the smaller CF (Table 1). The ability of activators such as **3** and **6** to mediate together with polyarginine the release of the large CFD from vesicles suggested the involvement of mechanisms other than carrier type,[36] *e.g.*, leakage through transient bilayer defects (compare with below DPPC experiments). The different kinetics observed for coronene and pyrene butyrates **3** and **6** hinted at the possibility that different activators may act by different mechanisms (Fig. 6Aa and c).

Table 2 Characteristics of coronene activators in EYPC-LUVs⊃CF at constant lipid concentration as a function of carrier concentration[a]

Entry	Anion[b]	pR/nM[g]	Y_{MAX} (%)[c,d]	EC_{50}/μM[c,e]	E[f]
01	**3**	250	65 ± 2	4.3 ± 0.3	7.5
02	**3**	125	51 ± 2	3.3 ± 0.2	6.1
03	**3**	50	43 ± 2	2.6 ± 0.2	5.4
04	**4**	250	50 ± 3	7.5 ± 0.7	5.2
05	**4**	125	42 ± 1	7.6 ± 0.2	4.3
06	**4**	50	22 ± 1	4.6 ± 0.1	2.5

[a] As in Table 1; measured at 25 °C. [b] As in Table 1. [c] As in Table 1. [d] As in Table 1. [e] As in Table 1. [f] As in Table 1. [g] pR, poly-L-arginine.

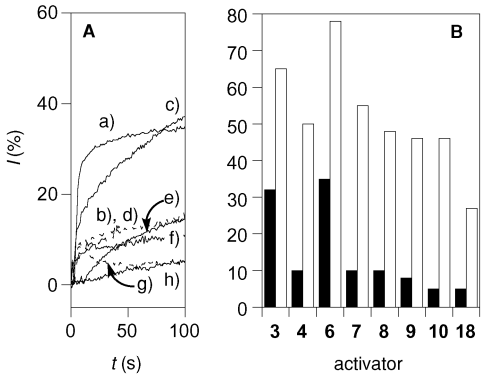

Fig. 6 (A) CF-dextran (CFD) efflux from EYPC-LUVs⊃CFD in the presence of pR (250 nM) and activators **3** (a, 20 μM), **4** (b, 10 μM), **6** (c, 100 μM), **7** (d, 15 μM), **8** (e, 20 μM), **9** (f, 6 μM), **10** (g, 5 μM) and **18** (h, 30 μM, procedure as in Fig. 4), measured at 25 °C. (B) Comparison of CF emission obtained for CF (□, Table 1) and CFD efflux (■, A) mediated by $pR\cdot(X)_{m'}\cdot(\mathbf{Y})_{m''}$ complexes at saturation with activators **Y**.

2.2 Activator–membrane interactions

The main phase transition of DPPC-LUVs⊃CF occurs at 41.4 °C.[62] Maximal efficiencies and EC_{50}'s of pertinent activators such as fullerene (**1**), coronene (**3**), pyrene (**6**) and calixarene (**10, 12**) carboxylates plus cholesterol sulfate **20** were determined below and above this temperature (Table 3). Efficiencies of all tested activators decreased with decreasing membrane fluidity. Whereas the EC_{50}–T profile showed less significant changes (Fig. 7B), the Y_{MAX}-T profile for pyrene sulfate **9** as representative activator exhibited the expected continuous increase with increasing temperature (Fig. 7A).

Table 3 Characteristics of selected anion activators in DPPC-LUVs⊃CF at constant lipid and carrier concentration as a function of temperature[a,h]

Entry	Anion[b]	T/°C[i]	Y_{MAX} (%)[c,d]	EC_{50} (μM)[c,e]	E[f]
01	**1**	25	—[g]	>100	0.0
02	**1**	60	40 ± 3	0.098 ± 0.007	7.8
03	**3**	25	70 ± 1	5.8 ± 0.1	7.6
04	**3**	60	83 ± 2	1.7 ± 0.1	11.2
05	**6**	25	65 ± 1	57 ± 1	3.9
06	**6**	60	91 ± 3	43 ± 2	6.0
07	**9**	25	18 ± 1	3.0 ± 0.3	2.2
08	**9**	60	48 ± 2	4.7 ± 0.6	5.4
09	**10**	25	—[g]	>100	0.0
10	**10**	60	79 ± 2	0.80 ± 0.04	11.9
11	**12**	25	29 ± 1	38 ± 1	2.0
12	**12**	60	90 ± 1	15 ± 1	8.0
13	**20**	25	3 ± 1	26 ± 1	0.3
14	**20**	60	51 ± 3	13 ± 1	4.7

[a] As in Table 1. [b] As in Table 1. [c] As in Table 1. [d] As in Table 1. [e] As in Table 1. [f] As in Table 1. [g] As in Table 1. [h] DPPC: dipalmitoyl phosphatidylcholine. [i] T: temperature.

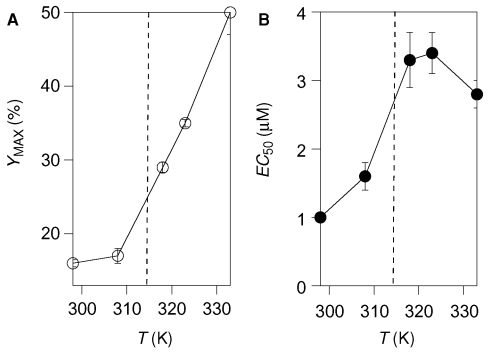

Fig. 7 (A) Y_{MAX} and (B) EC_{50} for pyrene sulfate **9** to activate pR (500 nM) in DPPC-LUVs⊃CF as a function of temperature. The dotted line indicates the phase transition of DPPC at 41.4 °C, data points were taken at 25, 35, 45, 50 and 60 °C.

The efficiency sequences in sol-phase DPPC, in gel-phase DPPC and in sol-phase EYPC were not the same (Table 3). The sequence fullerene > calix[4]arene ≈ coronene > pyrene in fluid-phase EYPC at 25 °C (Table 1) changed to coronene > calix[4]arene > fullerene > pyrene carboxylates in fluid-phase DPPC at 60 °C (Table 3). The exceptional efficiencies of coronene activator **3** and calix[4]arene activators **10** and **12** originated mainly from maximal activities $Y_{MAX} \geq 80\%$ (Table 3, entries 4 and 10). The EC_{50}'s of coronene **3** and calix[4]arene **10** in DPPC bilayers at 60 °C were slightly lower than those in EYPC bilayers at 25 °C.

Remarkably, the maximal activity of coronene-carrier complexes $\mathbf{R}_n{\cdot}(X)_{m'}{\cdot}(\mathbf{3})_{m''}$ in crystalline DPPC at 25 °C (Table 3, entry 3) exceeded that in liquid-crystalline EYPC at 25 °C slightly (Table 1, entry 3). This distinct DPPC > EYPC selectivity of coronenebutyrate **3** was complementary to fullerene activator **1** with maximal EYPC > DPPC selectivity (Table 3, entries 1 and 2 *versus* Table 1, entry 1). Overall, the efficiency sequence in crystalline DPPC bilayers at 25 °C was coronene > pyrene > calix[4]arene > fullerene carboxylates. Calix[4]arene **10** and fullerene **1** were completely inactive (Table 3, entries 1 and 9). High activities of coronenes and pyrenes in DPPC vesicles might relate to the preference of polyaromatic hydrocarbons to partition into liquid ordered phase rather than liquid disordered phase of a bilayer.[63,64] This sequence might also suggest that mechanisms other than a carrier mechanism[36] contribute to the activity of complexes $\mathbf{R}_n{\cdot}(X)_{m'}{\cdot}(\mathbf{Y})_{m''}$ with coronene and pyrene activators but, with all appropriate caution, presumably not to that of $\mathbf{R}_n{\cdot}(X)_{m'}{\cdot}(\mathbf{Y})_{m''}$ carriers with fullerene and calixarene activators. This interpretation was compatible with the results from CF-dextran efflux (Fig. 6).

Table 4 Characteristics of selected anion activators in EYPC-LUVs⊃CF at constant carrier concentration with and without cholesterol and ergosterol[a]

Entry	Anion[b]	Sterol[g]	Y_{MAX} (%)[c,d]	EC_{50}/μM[c,e]	E[f]
01	**1**	—	48 ± 1	0.051 ± 0.002	10.0
02	**1**	chol	37 ± 2	0.077 ± 0.007	7.4
03	**1**	erg	36 ± 2	0.070 ± 0.006	7.3
04	**3**	—	65 ± 2	4.3 ± 0.3	7.5
05	**3**	chol	52 ± 3	14 ± 1	4.7
06	**3**	erg	51 ± 3	15 ± 1	4.5
07	**6**	—	78 ± 2	44 ± 2	5.1
08	**6**	chol	47 ± 1	39 ± 1	3.2
09	**6**	erg	59 ± 1	43 ± 2	3.9
10	**9**	—	46 ± 2	2.2 ± 0.2	5.9
11	**9**	chol	35 ± 1	1.6 ± 0.1	4.7
12	**9**	erg	33 ± 1	1.7 ± 0.1	4.4
13	**10**	—	46 ± 3	1.2 ± 0.2	6.5
14	**10**	chol	61 ± 4	3.1 ± 0.4	7.4
15	**10**	erg	60 ± 3	6.3 ± 0.8	6.4
16	**12**	—	68 ± 2	3.1 ± 0.2	8.3
17	**12**	chol	68 ± 1	5.5 ± 0.1	7.5
18	**12**	erg	70 ± 1	5.4 ± 0.1	7.7
19	**20**	—	48 ± 1	9.2 ± 0.3	4.7
20	**20**	chol	43 ± 3	8.6 ± 0.7	4.3
21	**20**	erg	41 ± 2	9.1 ± 0.5	4.1

[a] As in Table 1; measured at 25 °C. [b] As in Table 1. [c] As in Table 1. [d] As in Table 1. [e] As in Table 1. [f] As in Table 1. [g] chol: 10 mol% cholesterol, erg: 10 mol% ergosterol, total EYPC concentration constant.

The synergistic activity of complexes $\mathbf{R}_n{\cdot}(X)_{m'}{\cdot}(\mathbf{Y})_{m''}$ did not depend much on the presence of cholesterol (enriched in mammals) and ergosterol (enriched in fungi)[65,66] in EYPC-LUVs⊃CF (Table 4). Activator efficiencies remained either nearly constant (calixarenes **10** and **12**) or decreased slightly. Reduced efficiencies may, in part, originate from the increased order of sterol-rich membranes. With respect to alternative modes of membrane recognition, folate (**21**) was of interest because folate receptors occur enriched at the surface of tumor cells.[67,68] No activity was found in sterol-free EYPC-LUVs⊃CF, presumably because the produced $pR{\cdot}(X)_{m'}{\cdot}(\mathbf{21})_{m''}$ complexes were too hydrophilic (Table 1, entry 21).

Taken together, the efficiency of activator–carrier complexes depended on membrane fluidity rather than composition. This trend was more pronounced for spherical (fullerenes, calixarenes) than for planar activators (coronenes, pyrenes). These results are in agreement with the preferential interfacial partitioning of aromatic amphiphiles, rather than molecular recognition within the hydrophobic core of the bilayer.

The relevance of anion activation of oligo/polyarginines to penetrate live cells was demonstrated previously by incubating HeLa cells with pyrenebutyrate **6** before addition of R_8-alexa, a fluorescently labeled octa-L-arginine.[9] According to flow cytometry detection after removal of the cell surface-adsorbed peptides by trypsin treatment, CPP uptake increased up to 4-times in the presence of pyrenebutyrate **6**. Measured under nearly identical conditions, the maximal increase of CPP uptake observed in the presence of less sterol-sensitive calix[4]arene **10** (maximal 1.5-fold increase, Fig. 8A) as well as the more sterol-sensitive, EYPC-selective fullerene carboxylate **1** (maximal 1.2-fold increase, Fig. 8B) were clearly below that of pyrenebutyrate **6**. At high concentrations, both activators became inhibitors of CPP uptake. The attractive implication that spherical activators, particularly fullerene **1**, may specifically mediate CPP-uptake in bacteria will be investigated in due course.

2.3. Activator–carrier interactions

In water, pyrenebutyrate complexes $pR{\cdot}(X)_{m'}{\cdot}(\mathbf{6})_{m''}$ exhibited characteristic excimer emission[49,50,69–72] at 470 nm with a maximal

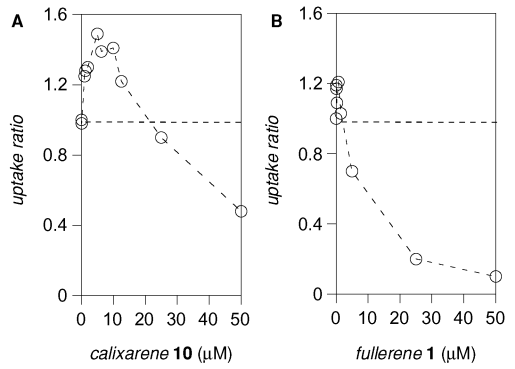

Fig. 8 Uptake ratios from flow cytometry for R_8-alexa by HeLa cells as a function of the concentration of activator **10** (A) and **1** (B) relative to activator-free uptake.

excimer/monomer ratio of E/M = 0.07.[1] This excimer emission increased for complexes pR·(X)$_{m'}$·(**7**)$_{m''}$ and pR·(X)$_{m'}$·(**8**)$_{m''}$ to a spectacular maximal E/M = 4.3 for complex pR·(X)$_{m'}$·(**9**)$_{m''}$ (Fig. 9 and Table 5).

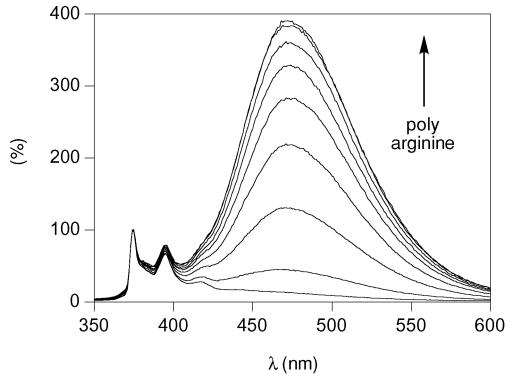

Fig. 9 Emission spectra of anion **9** (12 μM, λ_{ex} = 340 nm) in water in the presence of, with increasing intensity at 470 nm, 0, 50, 100, 150, 200, 250, 300, 350, and 400 nM pR (10 mM $Na_mH_nPO_4$, 107 mM NaCl, pH 7.4, 25 °C); normalized to monomer emission at 375 nm.

E/M ratios as well as EC_{50}'s decreased with decreasing concentration of activator–pR-complexes. E/M–pR profiles were recorded at the lowest detectable anion concentration to obtain thermodynamic data (Table 5). Despite the difference in the experiments, the obtained EC_{50}'s at high dilution and the EC_{50}'s obtained from function (Table 1) showed the same trend (**9** ≤ **8** < **7** < **6**). Taking the multivalent nature of the carrier into account, EC_{50} values obtained from the excimer emission (referring to pR concentration) and from functional studies (referring to anion concentration) are in good agreement.

Contrary to that of pyrene carboxylate **6**, the EC_{50} with respect to maximal excimer emission of pyrene sulfate **9** increased with increasing ionic strength (Fig. 10A). These differences suggested that ion pairing is dominant to the stability of the less efficient complexes with sulfate activators like pR·(X)$_{m'}$·(**9**)$_{m''}$, whereas hydrophobic interactions appear to contribute more significantly to the more efficient complexes with carboxylates like pyrene **6**.

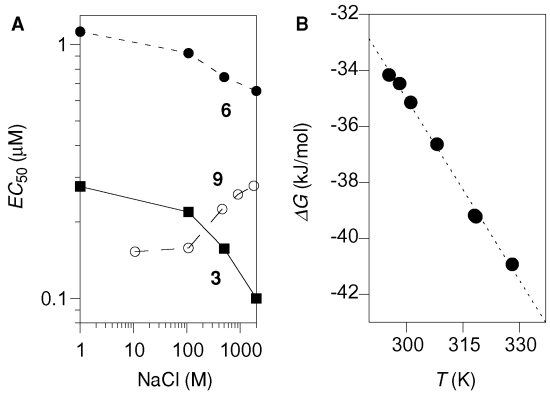

Fig. 10 Dependence of the formation of activator–pR complexes with pyrene carboxylate **6** (●), pyrene sulfate **9** (○) as well as coronene carboxylate **3** (■) on (A) ionic strength (at 25 °C) and (B) temperature (at 107 mM NaCl). EC_{50}'s and ΔG's were determined from Hill analysis of the changes in activator emission with increasing pR concentration as illustrated in Figs. 9 and 11.

This interpretation was supported by the dependence of complex pR·(X)$_{m'}$·(**6**)$_{m''}$ on temperature (Fig. 10B). As expected for the exchange of high-affinity phosphate counteranions with carboxylates of lower affinity,[39–45] complex formation was clearly endothermic (ΔH = +29.7 kJ mol^{-1}). Overcompensation of these losses by massive entropy gains corroborated the importance of desolvation of ions as well as large aromatic surfaces (TΔS = +64.2 kJ mol^{-1} at 25 °C).

Compared to the pyrene series, the emission spectra of activator–pR complexes with coronene **3** exhibited quite strong excimer emission,[69] reaching E/M ratios up to 28 (Fig. 11). Their "noisy" emission was indicative of scattering due to flocculation of the resulting complexes pR·(X)$_{m'}$·(**3**)$_{m''}$. Even stronger scattering was found in the emission spectra of the corresponding coronene sulfate complexes pR·(X)$_{m'}$·(**4**)$_{m''}$.

Table 5 Spectroscopic and thermodynamic data of activator–pR complexes for coronene and pyrene anions **3** and **5–9** in water[a]

Entry	Anion[e]	E/M[f]	EC_{50}/nM[g]
01	**3**	28.0[c], 1.36[d]	20.3 ± 1[d]
02	**5**	—[h]	—[h]
03	**6**	0.07[b]	920 ± 60[b]
04	**7**	0.65[b], 0.08[c],	150 ± 10[c]
05	**8**	1.90[b], 0.10[c]	122 ± 4[c]
06	**9**	4.27[b], 3.91[c], 1.88[d]	20.0 ± 1[d]

[a] From fractional changes in emission intensities at high (pyrenes, 375 nm; coronenes, 427 nm) and low energy (pyrenes, 470 nm; coronenes, ~500 nm) at constant anion concentration and varied pR concentration (107 mM NaCl, 10 mM $Na_mH_nPO_4$, pH 7.4, 25 °C). [b] Anion concentration 120 μM. [c] Anion concentration 12 μM. [d] Anion concentration 1.2 μM. [e] See Fig. 3 for structures. [f] Excimer/monomer emission ratio at saturation with pR (entry 1: Fig. 11, entry 6: Fig. 9). [g] Determined at minimal detectable anion concentration, from E/M-pR profiles, analyzed with eqns. (4)–(5), see experimental part. [h] No excimer emission observed.

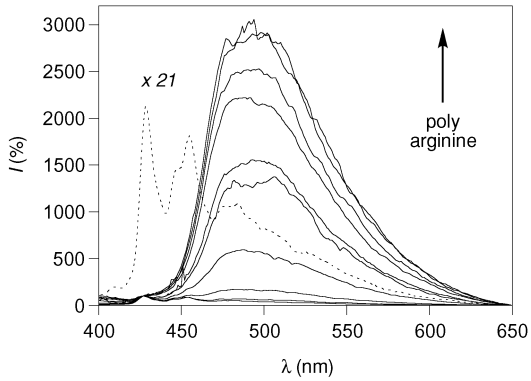

Fig. 11 Emission spectra of coronene carboxylate **3** (12 μM, λ_{ex} = 340 nm) in water in the presence of, with increasing intensity at ~500 nm, 0, 50, 100, 150, 200, 250, 500, 1200, 4000 and 5000 nM pR (10 mM $Na_mH_nPO_4$, 107 mM NaCl, pH 7.4), normalized to maximal monomer emission at 427 nm. Dotted spectrum: Magnified emission spectrum of **3** without pR (21×).

According to their excimer emission, the EC_{50}'s of coronenebutyrate complexes $pR\cdot(X)_{m'}\cdot(\mathbf{3})_{m''}$ decreased with increasing ionic strength (Fig. 10A, ■), nicely corroborating results with the corresponding pyrenebutyrate complexes $pR\cdot(X)_{m'}\cdot(\mathbf{6})_{m''}$, this decrease implied dominance of hydrophobic interactions in complexes with comparably weak carboxylate–guanidinium pairs (Fig. 10A, ■ and ●). The values at high ionic strength may contain contributions from self-assembly of coronene **3** observed under these conditions. Compared to that of pyrene carboxylate complex $pR\cdot(X)_{m'}\cdot(\mathbf{6})_{m''}$, the lower EC_{50} of coronene carboxylate complex $pR\cdot(X)_{m'}\cdot(\mathbf{3})_{m''}$ corroborated the increased activator affinity with increasing aromatic surface area (Table 5, entry 1 *versus* entry 3).

The excimer emission of pyrene–polyarginine complexes allowed us to detect the formation of "invisible" anion–pR complexes as well. The excimer emission of pyrene complex $pR\cdot(X)_{m'}\cdot(\mathbf{8})_{m''}$, for instance, decreased in the presence of increasing concentrations of calixarene **12** (Fig. 12). This change in emission reflected the transformation of the "visible" complex $pR\cdot(X)_{m'}\cdot(\mathbf{8})_{m''}$ into the "invisible" complex $pR\cdot(X)_{m'}\cdot(\mathbf{12})_{m''}$. Competition experiments with other anion activators gave analogous results and could be used, if desired, to determine global dissociation constants of any activator-carrier complex of interest.[73,74]

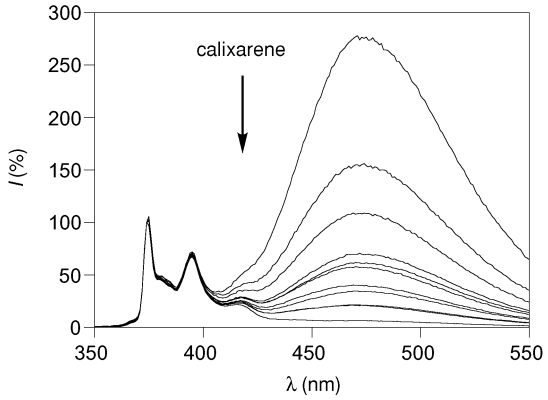

Fig. 12 Counteranion exchange assay for adaptable fluorometric detection of activator–carrier complexes like calix[4]arene complex $pR\cdot(X)_{m'}\cdot(\mathbf{12})_{m''}$. Emission spectra of anion **8** (120 μM, $\lambda_{ex} = 340$ nm) in water with pR (2.5 μM) and, with decreasing intensity at 470 nm, 0, 1, 1.5, 1.75, 2, 2.5, 3, 5, 10, 15 and 30 μM calixarene **12** (10 mM $Na_mH_nPO_4$, 107 mM NaCl, pH 7.4); normalized to maximal monomer emission at 375 nm.

Overall, the outcome of spectroscopic studies of complexes $pR\cdot(X)_{m'}\cdot(\mathbf{Y})_{m''}$ detected by excimer emission of pyrene and coronene activators confirmed that higher aromatics improve and high-affinity ion pairing weakens activator efficiency. The difference between the poor sulfate and the good carboxylate activators turned out to originate indeed from the dominant strong ion pairing which probably slows the anion exchange in the former, and the availability of supportive interactions such as hydrophobic contacts in the latter. This result supported the importance of arene-templated ion-pairing for function on the structural level. The increase in complex stability with increasing aromatic surface from pyrene to coronene revealed the importance of non-interfering remote contacts, *i.e.*, interactions far from the active site,[48] to support arene-templated ion pairing[38] without loss in activity. The two carboxylates positioned above an extended π-surface of the best activator, *i.e.*, the Bingel fullerene **1**, appear perfectly preorganized for arene-templated ion pairing (Fig. 13B). Possibilities for remote contributions to complex stability include additional association of guanidinium cations on the extended aromatic surfaces,[75] π–π interactions between proximal activators, and so on.

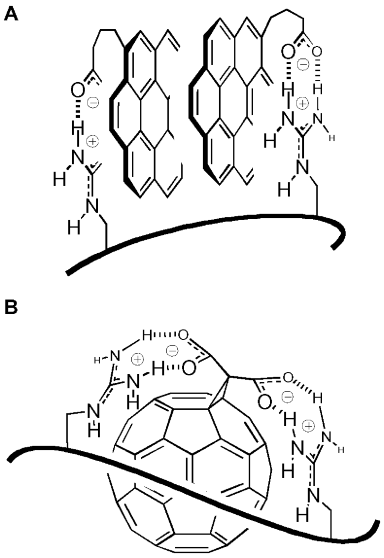

Fig. 13 Arene-templated ion pairing exemplified with notional structures of activator–carrier complexes $pR\cdot(X)_{m'}\cdot(\mathbf{3})_{m''}$ (A) and $pR\cdot(X)_{m'}\cdot(\mathbf{1})_{m''}$ (B); additional possibilities like binding of phosphate–guanidinium pairs on π-surfaces are not depicted.

3 Summary and conclusions

The objective of this study was to elaborate on the nature and selectivity of the interactions of selected anion activators with polyarginine (pR) carriers on the one hand and lipid bilayer membranes on the other hand. We found that activator–membrane interactions are dominated by the physical properties of the bilayer membrane with little recognition of specific components like ergosterol or cholesterol. This result was consistent with interface-directed translocation[28,29] as one possible origin of the superb activator efficiency of higher aromatics like amphiphilic fullerenes, calixarenes and coronenes. Reduced dependence on membrane fluidity and on the size of the transported anion with planar coronene and pyrene compared to spherical fullerene and calix[4]arene activators suggested more significant contributions from mechanisms other than carriers with the former. In HeLa cells, planar pyrenes were clearly more efficient CPP-activators than spherical fullerenes and calixarenes, a trend that might be reversed in bacteria.

Ideally, activators should bind tightly to carriers without sacrificing the anion exchange ability to retain carrier activities. Efficient activators are shown to fulfil this requirement with large aromatic surfaces for, presumably, arene-templated carboxylate–guanidinium pairing[38] stabilized by multiple interactions remote[48] from the active sites. Maybe accounting for interface-directed translocation as well, arene-templated ion pairing supported by remote contacts on large surfaces seems to reach perfection with fullerene **1** (Fig. 13B). The spectacular spectroscopic characteristics discovered for certain activator–carrier complexes open attractive perspectives with regard to sensing applications.

4 Experimental

4.1 Materials

Poly-L-arginine (HCl salt, MW 14 000, DP 72), sodium dodecyl sulfate (SDS), triton X-100, buffers and salts were purchased from Sigma, 4-pyrene-1-yl-butyric acid from Acros Organics, coronene from Aldrich, fullerene C_{60} from Alfa Aesar, egg yolk phosphatidylcholine (EYPC) and dipalmitoyl phosphatidylcholine (DPPC) from Avanti, cholesterol sulfate from Northern Lipids, mono-*n*-dodecylphosphate from Lancaster and reagents for synthesis, 5(6)-carboxyfluorescein (CF), 2-pyrene-1-yl-acetic acid, 6-pyrene-1-yl-caproic acid, cholesterol, ergosterol and lauric acid from Fluka. All reactions were performed under

N_2 or argon atmosphere. Column chromatography was carried out on silica gel 60 (Fluka, 40–63 μm), reverse phase column chromatography on ODS (Fluka Silicagel 100 C18-Reverse Phase), analytical thin layer chromatography (TLC) on silica gel 60 (Fluka, 0.2 mm) and preparative TLC (PTLC) on silica gel GF (Analtech, 1000 μm). Melting points (mp) were recorded on a heating table from Reichert (Austria). ESI-MS and APCI-MS were performed on a Finnigan MAT SSQ 7000 instrument. ^{1}H and ^{13}C spectra were recorded (as indicated) on either a Bruker 300 MHz, 400 MHz or 500 MHz spectrometer and are reported as chemical shifts (δ) in ppm relative to TMS ($\delta = 0$). Spin multiplicities are reported as a singlet (s), doublet (d), triplet (t), with coupling constants (J) given in Hz, or multiplet (m). ^{1}H and ^{13}C resonances were assigned with the aid of additional information from 2D NMR spectra (H,H-COSY, DEPT 135, HSQC and HMBC). UV-Vis spectra were measured on a Varian Cary 1 Bio spectrophotometer. Fluorescence measurements were preformed on either a FluoroMax-2 or a FluoroMax-3, Jobin Yvon-Spex. The Mini-Extruder with a polycarbonate membrane, pore size 100 nm, used for LUV preparation was from Avanti.

Abbreviations. CF: 5(6)-carboxyfluorescein; DBU: 1,8-diazabicyclo[5.4.0]undec-7-ene; DIPEA: *N*,*N*′-diisopropylethylenediamine; DMAP: 4-dimethylaminopyridine; DMF: *N*,*N*-dimethylformamide; EYPC-LUVs: egg yolk phosphatidylcholine large unilamellar vesicles; TBDPS: tetrabutyldiphenylsilyl; THF: tetrahydrofuran.

4.2 Synthesis

Anion activators **1, 3, 8–15** and **19** were prepared following previously reported procedures.[9,51,58,60] Stock solutions were prepared for all anions in buffer except for **1** and **2** (DMSO–water 1 : 1) and **3** and **4** (DMSO/water 9 : 1). The pH of all stock solutions was measured and accurately adjusted if necessary; concentrations were confirmed, if applicable, by UV/vis spectroscopy (if applicable).

4.2.1 Fullerene disulfate 2 (disodium salt). This compound was prepared in overall five steps as outlined in Scheme 1.

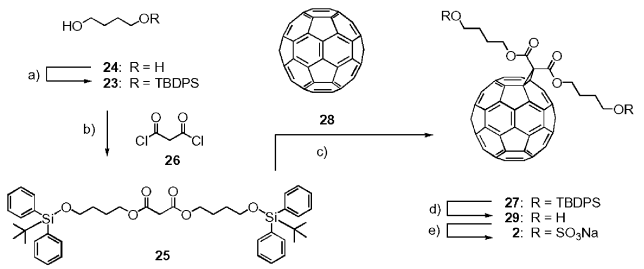

Scheme 1 Conditions: a) TBDPSCl, DIPEA, CH_2Cl_2, rt, 2 h, 95%; b) **26**, pyridine, DMAP, THF, rt, 12 h, 71%; c) **28**, I_2, DBU, toluene, rt, 12 h, 26%; d) AcOH, Bu_4NF, THF, rt, 16 h, 62%; e) 1. $ClSO_3H$, ether, 0 °C, 10 min, 2. NaOH, 80%.

*4-(tert-Butyl-diphenyl-silanyloxy)-butan-1-ol **23**.* To a solution of **24** (5.0 g, 55 mmol) in CH_2Cl_2 (10 ml) containing DIPEA (10 ml), TBDPSCl (5 ml, 18 mmol) was added dropwise at room temperature. The solution was stirred for 2 hours, concentrated *in vacuo* and purified by column chromatography (hexane–EtOAc 10 : 1, $R_f = 0.8$) to give **23** (5.63 g, 95%) as a colorless oil. ^{1}H NMR (400 MHz, $CDCl_3$): δ 7.74 (d, ^3J (H,H) = 7.8 Hz, 4H), 7.60–7.40 (m, 6H), 3.76 (t, ^3J (H,H) = 5.8 Hz, 2H), 3.72 (t, ^3J (H,H) = 5.8 Hz, 2H), 2.20 (broad s, 1H, exchange with D_2O), 1.80–1.69 (m, 4H), 1.12 (s, 9H); ^{13}C NMR (100 MHz, $CDCl_3$): δ 135.6 (d), 133.7 (s), 129.7 (d), 127.7 (d), 67.0 (t), 62.9 (t), 29.9 (t), 29.3 (t), 26.9 (q), 19.2 (s); MS (ESI, MeOH): m/z (%) 330 (100) $[M + H]^+$.

*Malonic acid bis-[4-(tert-butyl-diphenyl-silanyloxy)-butyl] ester **25**.* To a solution of **23** (2.0 g, 6.1 mmol), pyridine (520 μl, 6.4 mmol) and DMAP (4.0 mg, 33 μmol) in dried THF and malonyl chloride **26** (296 μl, 3.0 mmol) were added at room temperature. The mixture was stirred overnight. After evaporation of THF, CH_2Cl_2 (20 ml) was added, and the organic layer was washed with water (20 ml), dried over $MgSO_4$, concentrated *in vacuo* and purified by column chromatography (CH_2Cl_2–MeOH 20 : 1, $R_f = 0.7$) to give **25** (1.56 g, 71%) as a yellow oil. ^{1}H NMR (400 MHz, $CDCl_3$): δ 7.71 (d, ^3J (H,H) = 7.6 Hz, 8H), 7.40–7.30 (m, 12H), 4.09 (t, ^3J (H,H) = 6.6 Hz, 4H), 3.59 (t, ^3J (H,H) = 6.3 Hz, 4H), 3.26 (s, 2H), 1.69 (tt, ^3J (H,H) = 6.6 Hz, ^3J (H,H) = 8.3 Hz, 4H), 1.53 (tt, ^3J (H,H) = 6.3 Hz, ^3J (H,H) = 8.3 Hz, 4H), 1.11 (s, 18H); ^{13}C NMR (100 MHz, $CDCl_3$): 166.7 (s), 135.6 (d), 133.9 (s), 129.7 (d), 127.7 (d), 65.5 (t), 63.3 (t), 28.9 (t), 28.3 (t), 26.9 (q), 25.1 (t), 19.3 (s); MS (ESI, MeOH): m/z (%) 726 (100) $[M + H]^+$.

*Fullerene **27**.* To a solution of **28** (50 mg, 69.4 μmol), **25** (55 mg, 76 μmol) and I_2 (22 mg, 86 μmol) in dried toluene (100 ml), DBU (27 μl, 170 μmol) was added. The mixture was stirred for 12 hours at room temperature. After evaporation of toluene, the crude product was filtered through a short plug of silica, eluting first with toluene (to remove unreacted **28**) and then with CH_2Cl_2. Purification by PTLC (petroleum ether–EtOAc 10 : 1, $R_f = 0.5$) gave pure compound **27** (26 mg, 26%) as a gummy oil. ^{1}H NMR (400 MHz, $CDCl_3$): δ 7.58 (d, ^3J (H,H) = 7.6 Hz, 8H), 7.40–7.25 (m, 12H), 4.42 (t, ^3J (H,H) = 6.6 Hz, 4H), 3.63 (t, ^3J (H,H) = 6.6 Hz, 4H), 1.86 (tt, ^3J (H,H) = 7.8 Hz, ^3J (H,H) = 6.6 Hz, 4H), 1.63 (tt, ^3J (H,H) = 6.6 Hz, ^3J (H,H) = 7.8 Hz, 4H), 1.00–0.98 (m, 18H); ^{13}C NMR (100 MHz, $CDCl_3$): δ 162.6 (s), 144.3 (s), 144.2 (s), 144.1 (s), 144.1 (s), 143.9 (s), 143.7 (s), 143.6 (s), 142.9 (s), 142.0 (s), 142.0 (s), 142.0 (s), 141.1 (s), 140.9 (s), 137.9 (s), 134.5 (d), 132.7 (s), 128.6 (d), 126.7 (d), 70.6 (s), 66.3 (t), 62.1 (t), 51.3 (s), 27.9 (t), 25.9 (q), 24.2 (d), 18.2 (s); MS (ESI, CH_2Cl_2): m/z (%) 1443 (45) $[M + H]^+$, 722 (100) $[M + 2H]^{2+}$, 721 (10) $[C_{60} + H]^+$.

*Fullerene diol **29**.* A solution of **27** (25 mg, 17 μmol) in THF (3 ml) was treated successively with acetic acid (20 μl, 0.35 mmol) and tetrabutylammonium fluoride (1 M in THF, 350 μL, 0.35 mmol) at room temperature. After stirring for 16 hours, the reaction mixture was diluted with $CHCl_3$–MeOH 1 : 1 (40 ml), washed with water (20 ml), dried over $MgSO_4$, concentrated *in vacuo* and purified by column chromatography (CH_2Cl_2–MeOH 8 : 1 then 4 : 1, $R_f = 0.6$) to give pure **29** (10 mg, 62%) as a brown oil. ^{1}H NMR (300 MHz, CD_3OD–$CDCl_3$): δ 4.05 (t, ^3J (H,H) = 6.4 Hz, 4H), 3.55 (t, ^3J (H,H) = 6.3 Hz, 4H), 1.70–1.55 (m, 4H), 1.55–1.40 (m, 4H); ^{13}C NMR (75 MHz, CD_3OD–$CDCl_3$): δ 163.6 (s), 145.3 (s), 145.3 (s), 145.2 (s), 144.7 (s), 144.6 (s), 143.9 (s), 143.0 (s), 143.0 (s), 142.2 (s), 141.9 (s), 141.0 (s), 139.0 (s), 129.0 (s), 71.6 (s), 63.4 (t), 61.6 (t), 29.3 (t), 26.2 (d); MS (ESI, CH_2Cl_2): m/z (%) 967 (100) $[M + H]^+$.

*Fullerene disulfate **2** (disodium salt).* Fullerene **29** (10 mg, 10 μmol) in anhydrous ether (4 ml) was added to chlorosulfonic acid (14 μl, 21 μmol) in anhydrous ether (2 ml) at 0 °C. The mixture was purged with nitrogen for an additional 30 minutes to remove HCl, diluted with water (4 ml), 1 M NaOH (to reach pH ~7) and isopropanol (5 ml), washed with hexane (2 × 5 ml) and concentrated *in vacuo*. Purification by reverse phase column chromatography (MeOH, $R_f = 0.5$) yielded **2** (9 mg, 80%) as a yellowish powder. mp: >230 °C; ^{1}H NMR (300 MHz, CD_3OD): δ 3.91 (t, ^3J (H,H) = 6.4 Hz, 4H), 3.79 (t, ^3J (H,H) = 6.3 Hz, 4H), 2.14 (tt, ^3J (H,H) = 6.4 Hz, ^3J (H,H) = 7.3 Hz, 4H), 1.89 (tt, ^3J (H,H) = 7.3 Hz, ^3J (H,H) = 6.3 Hz, 4H); ^{13}C NMR (75 MHz, CD_3OD): δ 163.6 (s), 145.3 (s), 145.3 (s), 145.2 (s), 145.2 (s), 144.7 (s), 144.6 (s), 143.9 (s), 143.1 (s), 143.1 (s), 142.2 (s), 141.9 (s), 140.9 (s), 139.0 (s), 128.2 (s), 71.6 (s), 64.9 (t), 63.4 (t), 49.8 (s), 23.6 (t), 21.9 (d); MS (ESI negative mode, MeOH); m/z (%) 1147 (100) $[M - Na]^-$, 562 (45), $[M - 2Na]^{2-}$.

4.2.2 4-Coronen-1-yl-butylsulfate 4 (sodium salt). This compound was prepared from 4-coronen-1-yl-butyric acid **3** in overall two steps.

4-Coronenyl-1-butanol. A solution of **3** (240 mg, 0.62 mmol) in THF (16 ml) was transferred slowly to a solution of $LiAlH_4$ (186 mg, 5.00 mmol) in THF (3 ml) at 0 °C. The mixture was stirred for 2 hours at 60 °C. The reaction mixture was cooled at 0 °C and water was added drop by drop. The reaction mixture was stirred for 20 min, filtered (washed with THF and CH_2Cl_2–MeOH) and concentrated *in vacuo*. Purification of the crude product by column chromatography (CH_2Cl_2, then CH_2Cl_2–EtOAc 10 : 1, $R_f = 0.4$) yielded 4-coronenyl-1-butanol (128 mg, 55%) as a yellow solid. Mp: 205.0–206.3 °C; IR: ν 3238 (m), 3019 (s), 1611 (s), 1461 (s), 1052 (s) cm^{-1}; ^1H NMR (400 MHz, DMSO-d_6): δ 9.24–9.00 (m, 10H), 8.93 (s, 1H), 4.46 (t, ^3J (H,H) = 5.3 Hz, 1H, exchange with D_2O), 3.79 (t, ^3J (H,H) = 7.9 Hz, 2H), 3.57 (dd, ^3J (H,H) = 6.4 Hz, ^3J (H,H) = 5.3 Hz, 2H), 2.13 (tt, ^3J (H,H) = 7.9 Hz, ^3J (H,H) = 7.5 Hz, 2H), 1.77 (tt, ^3J (H,H) = 7.5 Hz, ^3J (H,H) = 6.4 Hz, 2H); ^{13}C NMR (100 MHz, DMSO-d_6): δ 137.7 (s), 128.3 (s), 128.3 (s), 128.2 (s), 128.1 (s), 127.9 (s), 127.1 (s), 126.4 (d), 126.4 (d), 126.4 (d), 126.3 (d), 126.3 (d), 126.3 (d), 126.1 (d), 125.9 (d), 125.9 (d), 125.9 (d), 122.7 (d), 122.1 (s), 122.0 (s), 121.7 (s), 121.6 (s), 121.4 (s), 121.5 (s), 60.6 (t), 33.1 (t), 32.7 (t), 27.6 (t); MS (CI, DMF): m/z (%) 372 (100) $[M]^+$.

4-Coronen-1-yl-butylsulfate ***4*** *(sodium salt).* A solution of 4-coronenyl-1-butanol (91 mg, 0.24 mmol) in DMF (1.5 ml) was transferred slowly to a solution of chlorosulfuric acid (35 mg, 0.30 mmol) in THF (1.5 ml) at 0 °C. The mixture was stirred for 1 hour at room temperature and purged with nitrogen to remove HCl. The mixture was diluted with water (2 ml), 1 M NaOH (to reach pH ~7), water (50 ml) and 2-propanol (50 ml), washed with petroleum ether (2 × 30 ml) and concentrated *in vacuo*. Purification by reverse phase column chromatography (H_2O–acetone 1 : 1 $R_f = 0.6$, first with H_2O then to H_2O–acetone 5 : 1 to 3 : 1) yielded pure **4** (70 mg, 63%) as a yellow solid. mp: >230 °C. IR: ν 3467 (m), 3016 (s), 1613 (s), 1216 (s) cm^{-1}; ^1H NMR (400 MHz, DMSO-d_6): δ 9.22–9.00 (m, 10H), 8.94 (s, 1H), 3.91 (t, ^3J (H,H) = 6.5 Hz, 2H), 3.77 (t, ^3J (H,H) = 7.8 Hz, 2H), 2.13 (tt, ^3J (H,H) = 7.8 Hz, ^3J (H,H) = 7.2 Hz, 2H), 1.87 (tt, ^3J (H,H) = 7.2 Hz, ^3J (H,H) = 6.5 Hz, 2H); ^{13}C NMR (100 MHz, DMSO-d_6): δ 137.6 (s), 128.3 (s), 128.3 (s), 128.2 (s), 128.1 (s), 127.4 (s), 127.1 (s), 126.4 (d), 126.4 (d), 126.4 (d), 126.3 (d), 126.3 (d), 126.3 (d), 126.2 (d), 126.2 (d), 126.1 (d), 125.9 (d), 122.8 (d), 122.1 (s), 122.0 (s), 121.8 (s), 121.6 (s), 121.4 (s), 120.5 (s), 65.4 (t), 33.0 (t), 29.4 (t), 27.7 (t); MS (ESI negative mode, DMF): m/z (%) 451 (100) $[M - Na]^-$.

4.3 Vesicle preparation

Solutions of EYPC (for **EYPC-LUVs**), DPPC (for **DPPC-LUVs**), and mixtures of EYPC and either ergosterol (erg, for **EYPC/erg-LUVs**) or cholesterol (chol, for **EYPC/chol-LUVs**) (25 mg) in $CHCl_3$–MeOH 1 : 1 (2 ml) were dried under a stream of N_2 and then under vacuum (>2 h) to form thin films. The resulting films were hydrated with 1 ml buffer A (50 mM CF, 10 mM $Na_mH_nPO_4$, 10 mM NaCl, pH 7.4 (for **LUVs⊃CF**) or 7.4 mM CF-dextran, 7.4 mM HEPES, 37 mM NaCl, pH 7.4 (**EYPC-LUVs⊃CFD**)) for more than 30 min, subjected to freeze–thaw cycles (5×) and extrusions (15×, Mini-Extruder with two stacked polycarbonate membranes, pore size 100 nm). Extravesicular CF/CFD was removed by gel filtration (Sephadex G-50 for **LUVs⊃CF**, Sephacryl S300-HR for **LUVs⊃CFD**) with buffer B (10 mM $Na_mH_nPO_4$, 107 mM NaCl, pH 7.4). The LUV fractions were combined and diluted to 6 ml with buffer B. Lipid concentrations were estimated from amount of entrapped CF. The found values were in agreement with earlier results from phosphate analysis (due to 10 mM phosphate in the buffer, phosphate analysis did not give accurate results). The final stock solutions had the following characteristics: ~1.3 mM lipid; inside: 50 mM CF, 10 mM $Na_mH_nPO_4$, 10 mM NaCl, pH 7.4, (**LUVs⊃CF**) or 7.4 mM CFD, 7.4 mM HEPES, 37 mM NaCl, pH 7.4 (**LUVs⊃CFD**); outside: 10 mM $Na_mH_nPO_4$, 107 mM NaCl, pH 7.4.

4.4 Vesicle experiments

LUV stock solutions (1.3 mM lipid, above) were diluted with buffer (10 mM $Na_mH_nPO_4$, 107 mM NaCl, pH 7.4) to give ≈13 μM lipid, placed in a thermostated fluorescence cuvette (25 °C or as indicated) and gently stirred. CF efflux was followed at λ_{em} 517 nm (λ_{ex} 490 nm) as a function of time during the addition of anion activators at varied concentration (**1–22**, 20–40 μl from stock solutions, final concentrations as indicated), polyarginine (250 nM) and aqueous triton X-100 at the end of each experiment for calibration (0.024%). Data were normalized to fractional emission intensity I using eqn. (2)

$$I = (F_t - F_0)/(F_\infty - F_0) \quad (2)$$

where $F_0 = F_t$ at polyarginine addition, $F_\infty = F_t$ at saturation after lysis. Effective concentrations EC_{50} and Hill coefficients were determined by plotting the fractional activity Y (= I just before lysis) as a function of anion concentration and fitting them to the Hill eqn. (3)

$$Y = Y_0 + (Y_{MAX} - Y_0)/\{1 + (EC_{50}/c_{ANION})^n\} \quad (3)$$

where Y_0 is Y without anion, Y_{MAX} is a value with an excess anion at saturation, c_{ANION} is the anion concentration in cuvette and n is the Hill coefficient. Activator efficiencies E were calculated using eqn. (1), where Y_{MAX} is the maximal activity (%), EC_{50} the effective concentration (mM), and $f = 20.6$ an arbitrary scaling factor. Pertinent E, Y_{MAX}, and EC_{50} values are listed in Tables 1–4.

4.5 Flow cytometry with HeLa cells

The influence of counteranion **1** and **10** on the uptake of R_8-alexa by HeLa cells was determined using flow cytometry as described previously.[9] In brief, R_8-alexa was prepared by reacting H-$(Arg)_8$-Gly-Cys-NH_2 with 1.5 eq. alexa 488 C_5 maleimide (Molecular Probes) in DMF–MeOH (1 : 1, 1.5 h), purified with RP-HPLC and characterized by MALDI-TOFMS (calcd. 2126.4, found 2127.2). Human cervical cancer-derived HeLa cells (1.5×10^5 cells in 1.5 ml of α-MEM containing 10% (v/v) calf serum) were cultured on 60 mm dishes (48 h) and washed twice with PBS after removal of the medium. After incubation of the cells in the presence or absence of fullerene **1** or calixarene **10** (300 μl PBS, 5 min, 37 °C), addition of R_8-alexa (100 μl PBS, final peptide concentration 5 μM), incubation (15 min, 37 °C), washing (PBS, 3×), incubation with 0.01% trypsin (400 μl, 10 min, 37 °C), addition of PBS (600 μl) and centrifugation (2,000 rpm, 5 min), the cell pellet was suspended, washed (2 × 1 ml PBS) and finally resuspended in 1 ml of PBS for fluorescence analysis with a FACScalibur (BD Biosciences) flow cytometer using a 488 nm laser excitation and a 515–545 nm emission filter. Each sample was analyzed for 10 000 events.

4.6 Pyrene excimers

Solutions of pyrene anions **5–9** (0.12–120 μM) in buffer (2 ml, 10 mM $Na_mH_nPO_4$, 0–2 M NaCl, pH 7.4) were placed in a cuvette. Then, pR was added stepwise (concentrations appropriate to follow the appearance of excimer emission, see Table 5) and the solutions were gently mixed. Fluorescence emission spectra of the resulting solutions were measured with λ_{ex} 340 nm at 25–60 °C. The obtained spectra were normalized to maximal monomer emission intensity at 375 nm. E/M ratios $I^{EM} = I_{470}/I_{375}$ for given anions, NaCl concentrations and temperature were plotted as a function of pR concentration and analyzed using the eqn. (4)

$$I^{EM} = I_0{}^{EM} + (I_\infty{}^{EM} - I_0{}^{EM})/[1 + (EC_{50}/c)^n] \quad (4)$$

where I^{EM} is the response (relative excimer emission intensity), ${I_0}^{EM}$ the initial value, ${I_\infty}^{EM}$ the value at saturation, c the pR concentration, and n the Hill coefficient, to obtain EC_{50}'s. The calculated apparent K_D's (EC_{50}'s) were then plotted as a function of the concentration of NaCl (Fig. 10A) or, converted into ΔG using eqn. (5)

$$\Delta G = -RT\ln K_D \quad (5)$$

as a function of temperature ($R = 8.315$ J K^{-1} mol^{-1}, $T = 298$ K, Fig. 10B). Additional thermodynamic data were obtained using eqn. (6)

$$\Delta G = \Delta H - T\Delta S. \quad (6)$$

Data analysis was done with Kaleidagraph, version 3.5 (Synergy Software).

4.7 Pyrene excimers, anion competition assay

To solutions of pyrene sulfate **8** (120 μM) and anions **1, 2, 10–20** (appropriate concentration; c/μM) in buffer (2 ml, 10 mM $Na_mH_nPO_4$, 107 M NaCl, pH 7.4), pR (2.5 μM) was added. The solutions were gently mixed and the fluorescence emission spectra were measured with λ_{ex} 340 nm at 25 °C (**12**, Fig. 12). The obtained spectra were normalized as above and analyzed using the eqn. (7)

$$I^{EM} = {I_0}^{EM} + ({I_\infty}^{EM} - {I_0}^{EM})/[1 + (IC_{50}/c)^n] \quad (7)$$

analogous to eqn. (4) to obtain inhibitory constants $IC_{50} \pm$ error. Further analysis using the Cheng–Prusoff equation to estimate K_I values was possible.[73,74]

4.8 Coronene fluorescence

Solutions of coronene anion **3** (0.12–12 μM) in buffer (2 ml, 10 mM $Na_mH_nPO_4$, 100 mM NaCl, pH 7.4) were placed in a cuvette. Then, pR was added stepwise and the solutions were gently mixed. Fluorescence emission spectra of the resulting solutions were measured with λ_{ex} 340 nm at 25 °C. The obtained spectra were normalized to maximal monomer emission intensity at 427 nm (Fig. 11) and analyzed as described for pyrenes.

Acknowledgements

We thank D. Jeannerat, A. Pinto and J.-P. Saulnier for NMR measurements, P. Perrottet and the group of F. Gülaçar for MS, and the Swiss NSF (including National Research Program "Supramolecular Functional Materials" 4047-057496, SM), Japan Science and Technology Agency (JST) (SF), Delta Proteomics (ANL) and the CNRS (AWC) for financial support.

References

1 N. Sakai and S. Matile, *J. Am. Chem. Soc.*, 2003, **125**, 14348–14356.
2 N. Sakai, T. Takeuchi, S. Futaki and S. Matile, *ChemBioChem*, 2005, **6**, 114–122.
3 L. Monticelli, K. M. Robertson, J. L. MacCallum and D. P. Tieleman, *FEBS Lett.*, 2004, **564**, 325–332.
4 Y. Jiang, A. Lee, J. Chen, V. Ruta, M. Cadene, B. T. Chait and R. MacKinnon, *Nature*, 2003, **423**, 33–41.
5 Y. Jiang, V. Ruta, J. Chen, A. Lee and R. MacKinnon, *Nature*, 2003, **423**, 42–48.
6 R. B. Bass, P. Strop, M. Barclay and D. C. Rees, *Science*, 2002, **298**, 1582–1587.
7 D. Terrone, S. Leung, W. Sang, L. Roudaia and J. R. Silvius, *Biochemistry*, 2003, **42**, 13787–13799.
8 J. B. Rothbard, T. C. Jessop, R. S. Lewis, B. A. Murray and P. A. Wender, *J. Am. Chem. Soc.*, 2004, **126**, 9506–9507.
9 F. Perret, M. Nishihara, T. Takeuchi, S. Futaki, A. N. Lazar, A. W. Coleman, N. Sakai and S. Matile, *J. Am. Chem. Soc.*, 2005, **127**, 1114–1115.
10 N. Sakai, N. Sordé, G. Das, P. Perrottet, D. Gerard and S. Matile, *Org. Biomol. Chem.*, 2003, **1**, 1226–1231.
11 S. Futaki, Arginine-rich Peptides, *Curr. Protein Pept. Sci.*, 2003, **4**, 87–157.
12 G. Dom, C. Shaw-Jackson, C. Matis, O. Bouffioux, J. J. Picard, A. Prochiantz, M. P. Mingeot-Leclercq, R. Brasseur and R. Rezsohazy, *Nucleic Acids Res.*, 2003, **31**, 556–561.
13 P. E. G. Thorén, D. Persson, E. K. Esbjörner, M. Goksör, P. Lincoln and B. Nordén, *Biochemistry*, 2004, **43**, 3471–3489.
14 A. Ziegler, X. L. Blatter, A. Seelig and J. Seelig, *Biochemistry*, 2003, **42**, 9185–9194.
15 H. Binder and G. Lindblom, *Biophys. J.*, 2003, **85**, 982–995.
16 K. Takeshima, A. Chikushi, K. Lee, S. Yonehara and K. Matsuzaki, *J. Biol. Chem.*, 2003, **278**, 1310–1315.
17 S. D. Krämer and H. Wunderli-Allenspach, *Biochim. Biophys. Acta*, 2003, **1609**, 161–169.
18 S. M. Fuchs and R. T. Raines, *Biochemistry*, 2004, **43**, 2438–2444.
19 P. E. G. Thorén, D. Persson, P. Isakson, M. Goksör, A. Onfelt and B. Nordén, *Biochem. Biophys. Res. Commun.*, 2003, **307**, 100–107.
20 D. Persson, P. E. G. Thorén, M. Herner, P. Lincoln and B. Nordén, *Biochemistry*, 2003, **42**, 421–429.
21 J. L. Zaro and W. C. Shen, *Biochem. Biophys. Res. Commun.*, 2003, **307**, 241–247.
22 D. Seebach, K. Namoto, R. Yogesh, Y. R. Mahajan, P. Bindschädler, R. Sustmann, M. Kirsch, N. S. Ryder, M. Weiss, M. Sauer, C. Roth, S. Werner, H.-D. Beer, C. Munding, P. Walde and M. Voser, *Chem. Biodiv.*, 2004, **1**, 65–97.
23 T. B. Potocky, A. K. Menon and S. H. Gellman, *J. Biol. Chem.*, 2003, **278**, 50188–50194.
24 J. P. Richard, K. Melikov, E. Vives, C. Ramos, B. Verbeure, M. J. Gait, L. V. Chernomordik and B. Lebleu, *J. Biol. Chem.*, 2003, **278**, 585–590.
25 G. Zuber, E. Dauty, M. Nothisen, P. Belguise and J.-P. Behr, *Adv. Drug Delivery Rev.*, 2001, **52**, 245–253.
26 A. D. Miller, *Curr. Med. Chem.*, 2003, **10**, 1195–1211.
27 E. Nakamura and H. Isobe, *Acc. Chem. Res.*, 2003, **36**, 807–815.
28 W. M. Yau, W. C. Wimley, K. Gawrisch and S. H. White, *Biochemistry*, 1998, **37**, 14713–14718.
29 M. Schiffer, C. H. Chang and F. J. Stevens, *Protein Eng.*, 1992, **5**, 213–214.
30 R. MacKinnon, S. L. Cohen, A. Kuo, A. Lee and B. T. Chait, *Science*, 1998, **280**, 106–109.
31 W. C. Wimley, *Curr. Opin. Struct. Biol.*, 2003, **13**, 404–411.
32 A. N. J. A. Ridder, S. Morein, J. G. Stam, A. Kuhn, B. de Kruijff and J. A. Killian, *Biochemistry*, 2000, **39**, 6521–6528.
33 M. R. R. De Planque, J. A. W. Kruijtzer, R. M. J. Liskamp, D. Marsh, D. V. Greathouse, R. E. Koeppe II, B. de Kruijff and J. A. Killian, *J. Biol. Chem.*, 1999, **274**, 20839–20846.
34 M. R. R. De Planque, B. B. Bonev, J. A. A. Demmers, D. V. Greathouse, R. E. Koeppe II, F. Separovic, A. Watts and J. A. Killian, *Biochemistry*, 2003, **42**, 5341–5348.
35 J. M. Sanderson and E. J. Whelan, *Phys. Chem. Chem. Phys.*, 2004, **6**, 1012–1017.
36 S. Matile, A. Som and N. Sordé, *Tetrahedron*, 2004, **60**, 6405–6435.
37 G. W. Gokel and A. Mukhopadhyay, *Chem. Soc. Rev.*, 2001, **30**, 274–286.
38 S. E. Thompson and D. B. Smithrud, *J. Am. Chem. Soc.*, 2002, **124**, 442–449.
39 K. A. Schug and W. Lindner, *Chem. Rev.*, 2005, **105**, 67–114.
40 K. Ariga and T. Kunitake, *Acc. Chem. Res.*, 1998, **31**, 371–378.
41 M. D. Best, S. L. Tobey and E. V. Anslyn, *Coord. Chem. Rev.*, 2003, **240**, 3–15.
42 P. Breccia, M. Van Gool, R. Perez-Fernandez, S. Martin-Santamaria, F. Gago, P. Prados and J. de Mendoza, *J. Am. Chem. Soc.*, 2003, **125**, 8270–8284.
43 M. Berger and F. P. Schmidtchen, *J. Am. Chem. Soc.*, 1999, **121**, 9986–9993.
44 X. Salvatella, M. W. Peczuh, M. Giarí, R. K. Jain, J. Sánchez-Quesada, J. de Mendoza, A. D. Hamilton and E. Giralt, *Chem. Commun.*, 2000, 1399–1400.
45 B. P. Orner, X. Salvatella, J. Sánchez-Quesada, J. de Mendoza, E. Giralt and A. D. Hamilton, *Angew. Chem., Int. Ed.*, 2002, **41**, 117–119.
46 R. A. Kumpf and D. A. Dougherty, *Science*, 1993, **261**, 1708–1710.
47 J. P. Gallivan and D. A. Dougherty, *Proc. Natl. Acad. Sci. U. S. A.*, 1999, **96**, 9459–9464.
48 F. M. Menger, *Biochemistry*, 1992, **31**, 5368–5373.
49 O. T. Jones and A. G. Lee, *Biochemistry*, 1985, **24**, 2195–2202.
50 J. Martins and E. Melo, *Biophys. J.*, 2001, **80**, 832–840.
51 C. Bingel, *Chem. Ber.*, 1993, **126**, 1957–1959.
52 I. Lamparth and A. Hirsh, *J. Chem. Soc., Chem. Commun.*, 1994, 1727–1728.
53 S. Foley, C. Crowley, M. Smaihi, C. Bonfils, B. F. Erlanger, P. Seta and C. Larroque, *Biochem. Biophys. Res. Commun.*, 2002, **294**, 116–119.

54 C. Wang, L. A. Tai, D. D. Lee, P. P. Kanakamma, C. K.-F. Shen, T.-Y. Luh, C. H. Cheng and K. C. Hwang, *J. Med. Chem.*, 1999, **42**, 4614–4620.
55 H. Park, M. Chhowalla, Z. Iqbal and F. Sesti, *J. Biol. Chem.*, 2003, **278**, 50212–50216.
56 F. Rancan, S. Rosan, F. Boehm, A. Cantrell, M. Brellreich, H. Schoenberger, A. Hirsch and F. Moussa, *J. Photochem. Photobiol. B*, 2002, **67**, 157–162.
57 E. Da Silva, A. N. Lazar and A. W. Coleman, *J. Drug Delivery Sci. Technol.*, 2004, **14**, 3–20.
58 Davenport, B. Shen, T. W. Joseph and M. P. Straher, *Chem. Phys. Lipids*, 2001, **109**, 145–156.
59 C. T. Miller, R. Weragoda, E. Izbicka and B. I. Iverson, *Bioorg. Med. Chem.*, 2001, **9**, 2015–2024.
60 P. Talukdar, G. Bollot, J. Mareda, N. Sakai and S. Matile, *J. Am. Chem. Soc.*, in press.
61 S. Rex, *Biophys. Chem.*, 1996, **58**, 75–85.
62 P. Yeagle, *The Structure of Biological Membranes*, CRC Press, Boca Raton, Florida, 1992.
63 T. Baumgart, S. T. Hess and W. W. Webb, *Nature*, 2003, **425**, 821–824.
64 B. Hoff, E. Strandberg, A. S. Ulrich, D. P. Tieleman and C. Posten, *Biophys. J.*, 2005, **88**, 1818–1827.
65 B. De Kruijff and R. A. Demil, *Biochim. Biophys. Acta*, 1974, **339**, 57–70.
66 S. C. Hartsel and J. Bolard, *Trends Pharm. Sci.*, 1996, **17**, 445–449.
67 J. Turk, D. J. Waters and P. S. Low, *Cancer Lett.*, 2004, **213**, 165–172.
68 X. B. Zhao and R. J. Lee, *Adv. Drug. Delivery Rev.*, 2004, **56**, 1193–1204.
69 B. Stevens, *Spectrochim. Acta*, 1962, **18**, 439–448.
70 D.Y. Sasaki, *Cell Biochem. Biophys.*, 2003, **39**, 145–161.
71 B. C. Roy, B. Chandra, D. Hromas and S. Mallik, *Org. Lett.*, 2003, **5**, 11–14.
72 B.-B. Wang, X. Zhang, X.-R. Jia, Z.-C. Li, Y. Ji, L. Yang and Y. Wei, *J. Am. Chem. Soc.*, 2004, **126**, 15180–15194.
73 Y. Cheng and W. H. Prusoff, *Biochem. Pharmacol.*, 1973, **22**, 3099–3108.
74 H. C. Cheng, *Pharmacol. Res.*, 2004, **50**, 21–40.
75 R. B. M. Ansem and L. T. Scott, *J. Phys. Org. Chem.*, 2004, **17**, 819–823.